Advancements in Spectral Power Distribution Modeling of Light-Emitting Diodes

Benkner, Simon ; Herzog, Alexander ; Klir, Stefan; van Driel, Willem; Khanh, Tran Quoc

DOI
10.1109/ACCESS.2022.3197280

Publication date
2022

Document Version
Final published version

Published in
IEEE Access

IEEE Access
Multidisciplinary | Rapid Review | Open Access Journal

Received 28 June 2022, accepted 29 July 2022, date of publication 8 August 2022, date of current version 12 August 2022.

Digital Object Identifier 10.1109/ACCESS.2022.3197280

RESEARCH ARTICLE

Advancements in Spectral Power Distribution Modeling of Light-Emitting Diodes

SIMON BENKNER[1], ALEXANDER HERZOG[1], STEFAN KLIR[1], WILLEM D. VAN DRIEL[2], AND TRAN QUOC KHANH[1]

[1]Laboratory of Adaptive Lighting Systems and Visual Processing, Technical University of Darmstadt, 64289 Darmstadt, Germany
[2]Electronic Components, Technology and Materials Group, Faculty of Electrical Engineering, Delft University of Technology, 2628 CD Delft, The Netherlands

Corresponding author: Simon Benkner (benkner@lichttechnik.tu-darmstadt.de)

The contribution of European Union is acknowledged for supporting the study in the context of the Electronic Components and Systems for European Leadership Joint Untertaking (ECSEL JU) programme (2021-2024) under the grant #101007319. Additional information are available on: www.ai-twilight.eu.

ABSTRACT The unique radiative, photometric and colorimetric characteristic of a light-emitting diode is derived from its spectral power distribution. Modeling such characteristics with respect to the forward current, temperature or operating time has been subject of various studies. Deriving a simple analytical model, however, is not trivial due to the unique emission pattern varying with different types and technologies of light emitting diodes. For this purpose, curve fitting multiple superimposed Gaussian probability density functions to the spectral power distribution is a common approach. Despite excellent R^2 goodness of fit results, significant deviations within the photometric and colorimetric parameters, such as luminous flux or chromaticity coordinates, are observed. In addition, most studies were conducted on a small sample set of very few different spectral power distributions. This work provides a comprehensive comparison and evaluation of 19 different (superimposed) probability density function based models provided by the literature tested on a total of 15 different spectral power distributions of monochromatic blue, green and red light-emitting diode as well as phosphor-converted spectra of lime, purple and white samples with different correlated color temperatures. All models were evaluated by means of their coefficient of determination, radiant flux, chromaticity coordinate deviation and Bayesian Information Criterion. This study shows that a superimposed (split) Pearson VII model is able to outperform the commonly used Gaussian model approach by far. In addition, an application example in regard of forward current dependence is given to prove the proposed approach.

INDEX TERMS Light-emitting diode, LED, spectral power distribution, spectral modeling, spectral decomposition.

I. INTRODUCTION

The emission pattern of a light-emitting diode (LED) can be described by its spectral power distribution (SPD) $S(\lambda)$. Typical performance metrics such as the radiant and luminous flux Φ_e, Φ_v, CIE color coordinates, Correlated Color Temperature (CCT) or the Color Rendering Index (CRI) are derived from the SPD [1]. The shape of $S(\lambda)$ is formed by two main factors: First, the material parameters of the LED such as semiconductor material, number of quantum wells or the type of phosphor in case of a phosphor-converted (pc-)LED. Secondly, operating conditions impact the SPD by means of Drive Current I_F, Junction Temperature T_j, Ambient Temperature T_A, Humidity rH_A and operating time t. In order to investigate the influence of a specific material or operating parameter the SPDs behavior is modeled by means of this parameter. A popular modeling approach is deconvoluting the SPD in separate SPDs $S(\lambda) = \sum S_n(\lambda)$, such as $S_{Chip}(\lambda) + S_{Phosphor}(\lambda)$ for pc-LEDs. Using a superposition of multiple probability density functions (pdf) $S_n(\lambda) = f_{pdf}(x = \lambda)$ is a commonly used approach. Each separated SPD can then be further analyzed for example regarding its chromaticity

The associate editor coordinating the review of this manuscript and approving it for publication was Marcelo Antonio Pavanello.

shift and direction to identify underlying degradation mechanisms [2]. Real world SPD, however, exhibit pdf shapes with a certain skew. This either produces inaccuracies for a low number $S_n(\lambda)$ or results in an impractical high number of pdfs to ensure a certain accuracy.

The aim of this work is on finding a proper set of model functions for modeling the SPD of various monochromatic and pc-LEDs. Therefor, a review on existing modeling approaches is given. Afterwards a set of suitable model functions is evaluated on seven monochromatic and eight pc-LEDs. Subsequently the results are discussed and the optimized model function is implemented for an application example on simulating a monochromatic LEDs current dependency.

II. RELATED WORK

A. MONOCHROMATIC LED SPECTRA

The theoretical emission spectrum $I(E)$ of a monochromatic LED [3] is described by the product of the density of states $\rho(E)$ and carrier distribution allowed in the energy band described by the Boltzmann distribution $f_B(E)$ given in (1) with the Energy E, the Bandgap Energy E_g, Temperature T and Botzmann constant k_B.

$$I(E) \propto \rho(E) \cdot f_B(E) = \sqrt{E - E_g} \cdot e^{-\frac{E}{k_B T}} \tag{1}$$

Modeling the SPD by (1) requires in depth knowledge about the LEDs material parameters. Even then, due to variations in the manufacturing process and material composition as well as the physical construction of the LED package, it is difficult to give a sufficient estimate of the SPD. Reifegerste *et al.* [4] first proposed the idea of modeling a monochromatic LEDs spectral shape at different I_F and T_j by curve fitting different analytical functions to the SPD. For this purpose a set of ten functions was investigated on a single LED type. The functions are listed in table 2. It was concluded that a *Logistic Power Peak* model performed best on the studied LED sample. Contrary in [5] best results were yielded for an Asymmetric Double Sigmoidal (*Asym2Sig*) model on a blue, green and red LED sample. Keppens *et al.* [6] evaluated a Sum of *Gaussian* model on each two red, green and blue LED samples reporting a high coefficient of determination $R^2 > 0.97$ for five out of six LED samples. This study was extended with amber and red samples by Raypah *et al.* [7] reporting $R^2 > 0.95$. By approximating (1) with an infinite series expansion of *Power Law* model functions for both sides of the peak wavelength λ_p Mozyrska and Fryc [8] took a different approach. A $R^2 \approx 0.98$ could be realized on a deep blue 380 nm sample with a $R^2 \approx 0.99$ on a *Gaussian* model for as comparison. Current LEDs often utilize a multi quantum well (MQW) structure impacting the SPDs slope. For this purpose Vaskuri *et al.* [9], [10] reported suitable results for red and blue samples utilizing an *Asym2Sig* model. Since the scope of their work was on modeling junction temperatures no goodness of fit metrics were provided for a comparison to the studies above.

B. PHOSPHOR-CONVERTED LED SPECTRA

Analogous to monochromatic LEDs over the past decade advances in modeling pc-LEDs were reported. The following studies present exclusively white pc-LEDs since modeling color pc-LEDs (purple, amber, green/lime) has not been the scope of any study yet. A number of results on Sum of n *Gaussian* models with $n = 2..8$ superimposed pdfs have been reported. Guo *et al.* [11] separated the SPD in two narrow band (blue, red) and one wide band region (green). Subsequently, each region was modeled with two (narrow band) respectively four (wide band) totaling $n = 8$ weighted *Gaussian* model functions but no R^2 was reported. Similarly a combination of $n = 7$ unweighted *Gaussian* model was chosen by a R^2-maximizing algorithm by Song and Han [12]. On an $n = 2$ unweighted *Gaussian* model Chen *et al.* [13] achieved a $R^2 > 0.99$ on four different samples. Additional, [14], [15], [16], [17] focus on predicting certain performance parameters of white pc-LEDs by incorporating *Gaussian* models in their prediction algorithms denoting $R^2 > 0.98$ for the input fitting functions. Fan *et al.* yielded in their model SPD a minimal higher coefficient of determination for the *Asym2Sig* model compared to the *Gaussian* model of both $R^2 \approx 0.99$.

C. PHOTOMETRIC AND COLORIMETRIC ACCURACY VS. COEFFICIENT OF DETERMINATION

The majority of the above discussed studies present the coefficient of determination as a proper evaluation metric. From a mathematical or statistical point of view a $R^2 > 0.95$ may indicate a high correlation and thus a good result. Nonetheless some studies yield at best moderate results in the radiometric or colorimetric domain [5], [6], [7], [11], [15], [17], [18]. Therefore, a combination of statistical, colorimetric and radiometric parameters should be taken into account when selecting a proper model function.

III. EXPERIMENT

The following section emphasizes on describing the experimental details in regard of LED samples used, the investigated model functions and the implementation.

A. SAMPLES

A total of 15 different monochromatic (blue, green, red) and pc-LEDs (lime, purple, white) were selected to cover a diverse spectral range of SPDs within the visible light spectrum. Table 1 highlights the most important radiometric and colorimetric parameters. It should be noted, that the peak wavelengths for plateaus in the SPD were estimated to point out a distinct underlying function. The normalized SPDs are shown in Fig. 1.

B. IMPLEMENTATION

The experimental code is implemented in Python programming language with the LMFIT package [19] for model fitting and evaluation. For this purpose the built-in set of model

TABLE 1. Overview of LED sample key parameters: Radiant Flux Φ_e, Peak Wavelength(s) $\lambda_{p,n}$, CIE 1976 USC u', v'.

Sample	Φ_e (mW)	$\lambda_{p,n}$ (nm)	u' (a.u.)	v' (a.u.)
Blue 1	306.4	450.6	0.203	0.079
Blue 2	290.5	445.9	0.215	0.061
Blue 3	550.2	444.6	0.218	0.058
Green	184.7	518.9	0.054	0.571
Red 1	177.3	632.4	0.533	0.520
Red 2	336.5	633.4	0.537	0.519
Red 3	367.8	660.0	0.587	0.512
Lime	245.5	447.8; 541.1	0.187	0.558
Purple	363.3	447.6; 646.2	0.463	0.503
White 1	470.3	443.5; 515.7; 550.5; 650.9	0.220	0.482
White 2	214.6	443.3; 597.5	0.229	0.507
White 2700K	333.6	449.0; 461.7; 626.4	0.267	0.533
White 3000K	320.4	450.0; 461.6; 623.1	0.253	0.533
White 4000K	379.9	443.0; 547.0; 616.8	0.225	0.511
White 6500K	374.3	442.3; 536.1; 614.3	0.197	0.482

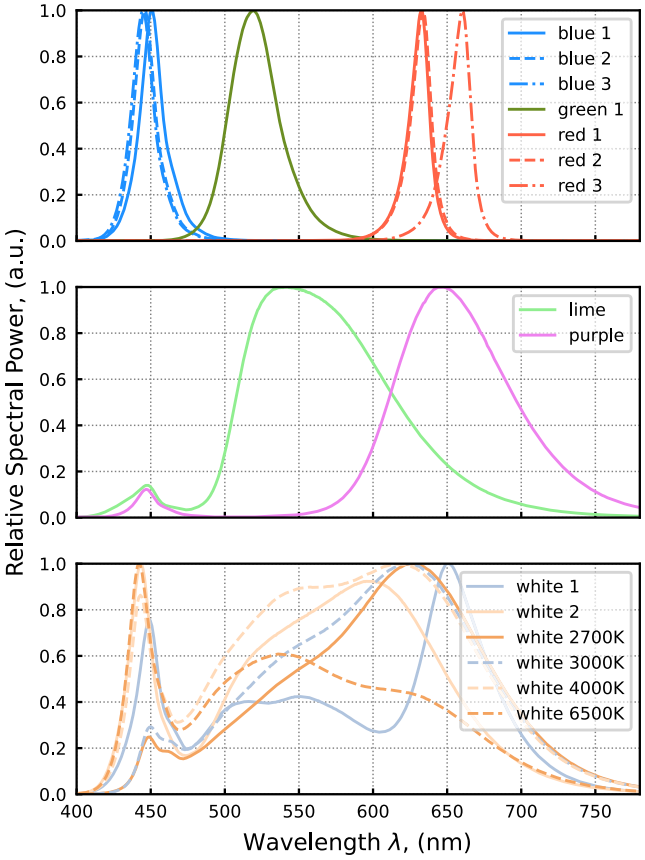

FIGURE 1. Peak wavelength intensity normalized test spectra of 15 sample LEDs: (top) monochromatic spectra of three blue, three red and one green led; (bottom) phosphor-converted spectra of four white, one lime and one purple led.

functions was extended by custom models according to the literature. Table 2 gives an overview of the evaluated models $f(\lambda, p)$ with their set independent variables $p = \{p_1, \ldots p_n\}$ as well as the literature reference for the model implementation. It should be noted, that two varying Pearson type VII models were found in the literature. Therefor, both implementation by Reifegerste *et al.* [4] and LMFIT built-in [19] are denoted

TABLE 2. Evaluated model functions for the experiment with their fitting parameters and the models literature reference.

Model	Independent Variables	Source
Gaussian	A, λ_p, σ	[4]–[8], [11]–[21]
Split Gaussian	$A, \lambda_p, \sigma_1, \sigma_2$	[4], [5]
Exponential Gaussian	A, λ_p, σ $\gamma \in [-100, 100]$	[19]
Skewed Gaussian	A, λ_p, σ $\gamma \in [-100, 100]$	[19]
Lorentzian 1. Ord.	A, λ_p, σ	[15], [16], [19]
Split Lorentzian 1. Ord.	$A, \lambda_p, \sigma_1, \sigma_2$	[19]
Lorentzian 2. Ord.	A, λ_p, σ	[4]
Asym. 2 Sigmoidal	A, λ_p, σ $S_1, S_2 \in [10^{-15}, 100]$	[4], [5], [9], [10], [16], [21]
Logistic Power Peak	A, λ_p, σ $S \in [10^{-15}, 100]$	[4], [5]
Asym. Power Peak	A, λ_p, σ $S \in [10^{-15}, 100]$	[4]
Pearson VIIa	A, λ_p, σ $S \in [10^{-15}, 100]$	[4]
Pearson VIIb	A, λ_p, σ $m \in [10^{-15}, 100]$	[19]
Split Pearson VII	$A, \lambda_p, \sigma_1, \sigma_2$ $S_1, S_2 \in [10^{-15}, 100]$	[4]
Voigt	A, λ_p, σ $\gamma = \sigma$	[19]
Pseudo Voigt	A, λ_p, σ $\alpha \in [10^{-15}, 100]$	[19]
Skewed Voigt	A, λ_p, σ $\gamma = \sigma$ $S \in [10^{-15}, 100]$	[19]
Moffat	A, λ_p, σ $\beta \in 10^{-15}, 100]$	[19]
Student T	A, λ_p, σ	[19]
Lognormal	A, λ_p, σ	[19]

Independent Variables: Amplitude A; Peak Wavelength λ_p; (left/right side) Standard Deviation $\sigma, \sigma_1, \sigma_2$; (left/right side) Skew/Kurtosis S, S_1, S_2; weighting or scaling parameter α, β, γ, m.

Pearson VIIa and Pearson VIIb respectively. The common model parameter boundaries were arbitrarily set to the following intervals: Amplitude $A \in [0.001, 100]$, Peak Wavelength $\lambda_p \in [400, 800]$, (left/right side) Standard Deviation $\sigma, \sigma_1, \sigma_2 \in [1, 300]$. Additional model specific parameter intervals can be found in table 2. All code is available at our repository: *https://github.com/SBenkner/Spectral-Fitting*.

Preliminary, two assumptions are made to find the most suitable fit function: The radiation pattern of a monochromatic LED follows only one type of model function. This function type can be superimposed $n_{\text{Chip}} \geq 1$ times to represent e.g. n different QW in a MQW structure. Secondly, pc-LEDs incorporate at least two superimposed functions $n = n_{\text{Chip}} + n_{\text{Phosphor}} \geq 2$ where $n_{\text{Chip}} \geq 1$ and $n_{\text{Phosphor}} \geq 1$. Since it can be assumed that $\lim_{n\to\infty} R^2 \to 1$ the number of model functions is limited to $n = 3$ for monochromatic LEDs and $n = 6$ for pc-LEDs to maintain a realistic and practical approach. Thus, with the given constraints the total number of possible model combinations can be calculated with $N(n) = M \cdot \sum_i^n i$ to $N_{\text{mono}}([1, 3]) = 57$ and $N_{\text{pc}}([2, 6]) = 95$ with $M = 19$ different model functions. The maximum number of fit iterations before the fit is aborted is set to 100.000. Each fit is evaluated regarding its statistical, radiometric and

colorimetric properties. In order to provide a comparability to the literature the coefficient of determination R^2 (2) has been selected from the statistical domain. Additionally, the fitted models Bayesian Information Criterion (BIC) was determined according to (3) with the number of data points m, the number of parameters k and the models maximum likelihood function $\hat{L}$ [22]. From the radiometric domain the relative difference in radiant flux $\Delta\Phi$ (4) was evaluated since even changes in brightness of about 7.4% are noticeable according to Hu and Davis [23]. To accompany a steadiness in the colorimetric perception the chromaticity difference $\Delta u'v'$ (5) [1] was chosen from the colorimetric domain since the CIE 1976 $u'v'$ color space is recommended by the CIE for its uniformity [24].

$$R^2 = \frac{\sum(y_{\mathrm{i,fit}} - \bar{y}_{\mathrm{true}})^2}{\sum(y_{\mathrm{i,true}} - \bar{y}_{\mathrm{true}})^2},$$
$$\bar{y}_{\mathrm{true}} = \frac{\sum_i^m y_{\mathrm{i,true}}}{N} \tag{2}$$
$$\mathrm{BIC} = k\ln(m) - 2\ln(\hat{L}) \tag{3}$$
$$\Delta\Phi = 100 \cdot \left(\frac{\Phi_{\mathrm{fit}}}{\Phi_{\mathrm{true}}} - 1\right) \tag{4}$$
$$\Delta u'v' = \sqrt{(u_{\mathrm{fit}} - u_{\mathrm{true}})^2 - (v_{\mathrm{fit}} - v_{\mathrm{true}})^2} \tag{5}$$

In order to delimit the set of possible models, boundaries have to be set for each singe metric (2)-(5) to rule out irrelevant models. Since, the coefficient of determination shows the correlation between the original and its fitted SPD a $R^2 \geq 0$ has to be expected. Values $R^2 < 0$ would indicate a negative correlation yielding an inverse shaped SPD fit of the original SPD. A difference in radiant flux of $\Delta\Phi < -100\%$ would represent a physically impossible negative SPD. Due to the high sensitivity of the human eye regarding a change of brightness the range of allowed difference in radiant flux was arbitrarily set to $\Delta\Phi \pm 25\%$. Considering the CIE 1976 UCS color space boundaries chromaticity difference values above $\Delta u'v' \approx 75 \times 10^{-3}$ would exceed the spectral locus. As described in [24] thresholds for $\Delta u'v'$ are mainly defined near the Planckian Locus of the CIE 1976 UCS color space diagram it is difficult to chose a specific threshold especially for monochromatic spectra. Thus, in this work the *CS4* threshold declared in IES/ANSI TM-35 [25] of $\Delta u'v' = 4 \times 10^{-3}$ is used.

IV. RESULTS AND DISCUSSION

Following, the different fit models results are presented and discussed with respect to their accuracy according to (2)-(5). First the results of the monochromatic set of SPDs are evaluated. Subsequently, the set of pc-LED spectra is analyzed.

In case of the monochromatic SPD samples 399 theoretical models in total were evaluated. Considering the above defined constraints a total of 174 models remained as valid for further inspection. Table 3 shows the number of valid functions for each sample and number of superimposed functions. As previous stated, the accuracy, and thus the number of valid models, increases with n. It can also be concluded that

TABLE 3. Total number of valid models for each sample and number of functions *n*.

Sample	$n=1$	$n=2$	$n=3$	$n=4$	$n=5$	$n=6$
Blue 1	1	2	9	-	-	-
Blue 2	5	6	12	-	-	-
Blue 3	5	6	12	-	-	-
Green	5	9	11	-	-	-
Red 1	1	3	10	-	-	-
Red 2	1	5	9	-	-	-
Red 3	2	3	8	-	-	-
Lime	-	5	11	12	13	12
Purple	-	0	0	5	8	7
White 1	-	0	7	6	10	11
White 2	-	9	14	13	11	14
White 2700K	-	10	14	14	15	14
White 3000K	-	6	14	14	14	12
White 4000K	-	3	12	10	10	11
White 6500K	-	5	10	12	13	15

even with $n = 1$ at least one model function can be found meeting the boundary conditions. Superimposing at least two functions yields a $\Delta u'v' < 2 \times 10^{-3}$ for all valid models.

Next, the top ten models with the lowest $\Delta u'v'$ of each sample SPD were compared. According to majority of the literature a composition of *Gaussian* models was expected to yield the best results. However, on the given monochromatic sample SPDs the *Gaussian* model was vastly underrepresented. A *(split) Pearson VII* distribution and *Skewed Voigt* model provided the lowest $\Delta u'v'$ and $\Delta\Phi$. The information gain from the coefficient of determination was rather small since all selected models showed a $R^2 \geq 0.98$. Taking $\Delta\Phi$ and BIC into account *(split) Pearson7* performed best overall on all monochromatic samples. It should be noted, that in most cases the LMFIT implemented *Pearson VIIb* model [19] performed slightly better that the other two *Pearson VII* models, yet all three *Pearson VII* models yielded superior results. A comparison of the *Pearson VII* and the *Gaussian* models for different n is given in table 4 and 5 for $\Delta u'v'$ and $\Delta\Phi$ respectively. In case of the red samples with a $n = 1$ *Gaussian* model the fit process exceeded the maximum fit iterations probably due to the chosen parameter boundaries in combination with the SPDs high right side skew an steep decrease. Therefore, no values can be reported. With only one *Pearson VII* type function 5 of 7 samples could meet the *CS4* condition while the remaining two samples slightly failed it by $\Delta u'v' < 0.51 \times 10^{-3}$. Whereas, the *Gaussian* models exceeded $\Delta u'v' < 10 \times 10^{-3}$. Even with $n = 3$ only 3 of 7 samples matched the *CS4* condition for the *Gaussian* model. An observable increase in $\Delta u'v'$ and $\Delta\Phi$ for $n = 2$ on sample Red 3 can be traced to a problem fitting two functions on the given type of SPD decreasing the fit quality compared to $n = 1$ due to *Gaussian* models missing kurtosis parameters.

By further analyzing the chromaticity coordinates offsets $u'_{\mathrm{orig}} - u'_{\mathrm{fit}}$, $v'_{\mathrm{orig}} - v'_{\mathrm{fit}}$ between the fitted SPDs and the original SPD as shown in fig. 2 two observations can be conducted: Firstly, the blue and red samples show a deviation towards the deep blue and deep red chromaticity coordinates respectively on the spectral locus. This is caused by a misalignment of the

TABLE 4. Chromaticity difference results of Pearson Type VII distribution (P7) compared to Gaussian distribution (G) with $n = 1..3$ model functions on the monochromatic LED set.

LED	$\Delta u'v'$ ($\times 10^{-3}$)					
	n=1		n=2		n=3	
	P7	G	P7	G	P7	G
Blue 1	4.04	16.78	1.00	8.88	1.21	5.06
Blue 2	0.73	12.08	2.38	5.99	0.51	4.75
Blue 3	1.44	11.54	2.00	5.79	0.32	4.62
Green	1.17	10.02	0.41	1.56	0.05	0.19
Red 1	2.55	-	2.20	7.32	0.07	2.51
Red 2	0.37	-	2.54	6.87	0.28	2.49
Red 3	4.51	-	10.15	16.93	0.37	3.53

TABLE 5. Difference in radiant flux results of Pearson Type VII distribution (P7) compared to Gaussian distribution (G) with $n = 1..3$ model functions on the monochromatic LED set.

LED	$\Delta\Phi$ (%)					
	n=1		n=2		n=3	
	P7	G	P7	G	P7	G
Blue 1	2.6	-8.1	-0.1	-1.4	0.0	-0.9
Blue 2	1.5	-7.5	0.4	-1.0	0.0	-1.0
Blue 3	1.2	-6.9	-0.3	-0.8	0.0	-0.9
Green	0.1	-3.8	0.1	-0.7	0.1	-0.2
Red 1	1.0	-	0.6	-2.0	0.1	-0.4
Red 2	1.3	-	0.7	-1.8	0.1	-0.4
Red 3	0.6	-	0.9	-7.8	-0.1	-0.4

λ_p parameter. Secondly, shape parameter(s) like σ of too high value result in a deviation towards green-yellow for the blue SPDs. A similar trend is emerges for the red 1 & 2 spectra towards yellow-green.

A similar procedure was performed for evaluating the pc-LED spectra. Out of the 760 evaluated models 406 models met the boundary conditions. Due to the varying shape of the phosphor-related spectral emissions a broader set of possible functions could be identified: *Gaussian*, *Split Gaussian*, *Skewed Gaussian*, *Asym2Sig*, *Pearson VIIa/b*, *Split Pearson VII*, *Skewed Voigt* and *Moffat*. The total number of valid functions for the pc-LED SPDs with respect to the number of superimposed functions is shown in tab. 3. Apart from the Purple and White 1 sample it was possible to find at least one model that met the *CS4* condition at $n = 2$ on every sample. Since White 1 was explicitly chosen because of its three phosphor peaks it was expected to fail. The purple sample on the other hand could not be fitted properly with low n because of the nature of its two separated peaks as further described at the end of this passage. In accordance to the monochromatic results described above the *(Split) Pearson VII* on average on all samples again yielded promising results as shown in tables 6 and 7. Especially at lower model numbers $n \leq 3$ *(Split) Pearson VII* outperforms a *Gaussian* model approach by a factor of at least more than two. Yet, with only two superimposed functions 5 of 8 samples can be sufficiently modeled with a *(Split) Pearson VII* model compared to only 1 of 8 models meeting the *CS4* condition with a *Gaussian* model. At higher model number of $n \geq 4$ both model types perform with a high accuracy. Further two special cases are observable: Firstly, the Purple and White 4000K samples

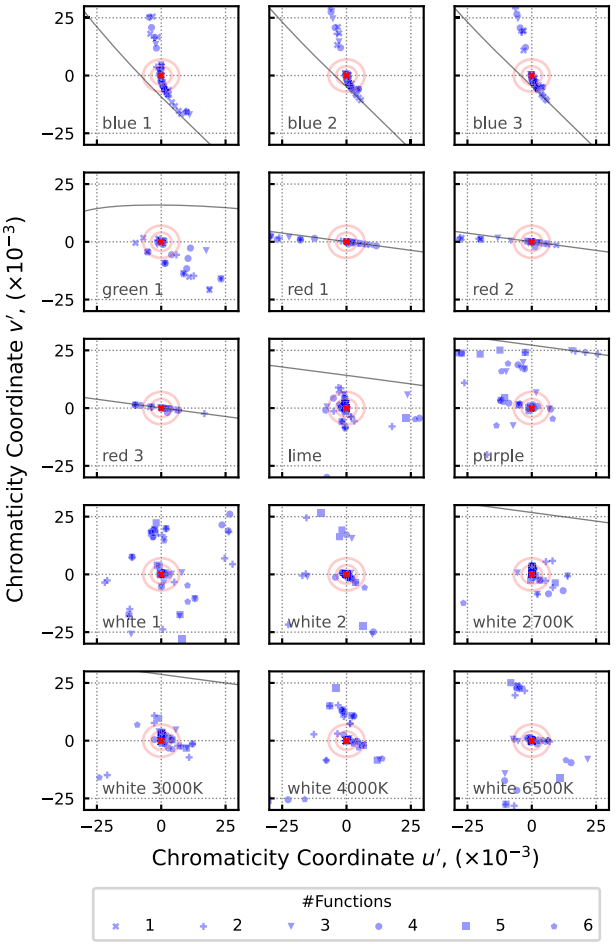

FIGURE 2. CIE 1976 chromaticity coordinate offset $u'_{orig} - u'_{fit}$, $v'_{orig} - v'_{fit}$ of each fit with respect to the original SPDs chromaticity coordinates for each sample SPD. The original SPDs chromaticity coordinate has been shifted to $u' = 0$ and $v' = 0$ (red x) for comparability. The *CS4* (inner red circle) and *CS7* (outer red circle) chromaticity deviation [25] are highlighted for better classification of the chromaticity deviation. Additional the shifted spectral locus (light gray line) shows the boundary of the CIE 1976 color space.

show an increase in $\Delta u'v'$ at $n = 6$ and $n = 5$ respectively for the *Gaussian* model that can be traced back to fitting problems analogous to the Red 3 sample. Secondly, both model types produce a high chromaticity difference for the Purple sample at $n = 2, 3$ as also observed in fig. 2. This situation occurs mostly due to the fact, that the fitting algorithm has to find a trade-off between magnitude and width of the resulting function alongside with a desired shape. For the given model types either the magnitude requirement is met by overfilling the valley between since the functions width exceeds the peak width. Alternatively, one or both peaks are underfilled since the shape/width requirements are satisfied with the drawback in magnitude.

The observed improvements of a *Pearson VII* type model compared to *Gaussian* one can be concluded due to two reasons: *(Split) Pearson VII* provides additional shape/skew adjustment capabilities given by its exponents m, S, S_1 and S_2. This allows a tighter fit to the semiconductor emission

TABLE 6. Chromaticity difference results of Pearson Type VII distribution (P7) compared to Gaussian distribution (G) with $n = 2..6$ model functions on the pc-LED set. The following abbreviations are used for the sample: W1=White 1, W2=White 2, WxxK=White xx00K.

LED	$\Delta u'v'$ ($\times 10^{-3}$)									
	n=2		n=3		n=4		n=5		n=6	
	P7	G	P7	G	P7	G	P7	G	P7	G
Lime	1.01	6.43	0.03	6.01	0.03	2.79	0.23	0.02	0.03	0.01
Purple	12.5	29.93	6.83	29.27	0.12	2.37	0.05	1.17	0.17	21.37
W1	6.07	25.61	1.18	0.84	0.17	0.61	0.20	0.61	0.13	0.6
W2	0.94	29.04	0.04	1.67	0.18	1.67	0.03	0.03	0.28	0.03
W27K	2.64	2.44	2.9	0.12	0.14	0.10	0.01	0.10	0.00	0.14
W30K	2.92	11.15	2.8	2.42	0.07	0.14	0.12	0.22	0.00	0.21
W40K	5.41	16.45	0.04	1.42	0.04	0.13	0.03	16.45	0.00	0.3
W65K	1.09	21.81	0.34	0.45	0.08	0.06	0.01	0.43	0.03	0.01

TABLE 7. Difference in radiant flux results of Pearson Type VII distribution (P7) compared to Gaussian distribution (G) with $n = 2..6$ model functions on the pc-LED set. The following abbreviations are used for the sample: W1=White 1, W2=White 2, WxxK=White xx00K.

LED	$\Delta\Phi$ (%)									
	n=2		n=3		n=4		n=5		n=6	
	P7	G	P7	G	P7	G	P7	G	P7	G
Lime	-0.4	-2.5	0.0	-2.3	0.0	0.3	0.1	-0.3	0.1	-0.1
Purple	-1.3	-3.1	1.2	-2.8	0.0	-0.3	0.1	0.0	0.0	-0.1
W1	0.7	1.3	0.5	-2.8	0.3	-0.2	0.2	-0.2	0.0	0.3
W2	0.9	-0.2	0.1	0.3	0.2	0.3	0.1	0.0	0.3	0.0
W27K	-0.4	0.5	0.4	-0.6	0.2	0.1	0.0	0.1	0.0	0.1
W30K	0.5	-0.2	0.8	0.5	0.1	-0.5	0.0	0.1	0.0	0.1
W40K	1.5	1.4	0.1	1.6	0.1	-0.2	0.1	1.4	0.0	0.1
W65K	1.0	2.0	0.4	-0.1	0.2	-0.1	0.1	0.3	0.1	-0.2

spectrum. Secondly, a *Gaussian* distribution is a special case of the *Pearson VII* distribution for large exponents $m, S, S_1, S_2 \to \infty$, thus, it approximates a *Gaussian* distribution at large numerical exponent values and covers the case of *Gaussian* like SPDs. Furthermore, result deviations between both *Pearson VIIa* [4] and *Pearson VIIb* [19] were observed, although both should theoretically yield the same results. The reason can be found in the different types of formulas Reifegerste *et al.* and Newville *et al.* provided. While *Pearson VIIb* appears to be the general form of Pearsons Type VII distribution, yet, no information or background on *Pearson VIIa* could be found. Both model functions *Pearson VIIa* and *Pearson VIIb* are shown in (6) and (7) respectively with the Beta-Function $\beta(a, b)$ set to $a = m - b$, $b = 0.5$ and $C = \left[\left(\lambda - \lambda_\mathrm{p}\right)/\sigma\right]^2$.

$$f_{\mathrm{PVIIa}}(\lambda; A, \lambda_\mathrm{p}, \sigma, S) = A \cdot \left[1 + C\left(2^{\frac{1}{S}} - 1\right)\right]^{-S} \quad (6)$$

$$f_{\mathrm{PVIIb}}(\lambda; A, \lambda_\mathrm{p}, \sigma, m) = A \cdot [\sigma\beta(a, b)]^{-1} [1 + C]^{-m} \quad (7)$$

It should be highlighted, that Reifegerste denotes the parameter S in *Pearson VIIa* and *Split Pearson VII* as a "skew"-parameter while the general form of a Pearson Type VII distribution is a symmetrical function only providing a "shape"-parameter m. Moreover, this might give an explanation to some rare cases of *Split Pearson VII* performing slightly worse than *Pearson VIIb* since an accuracy improvement should be observable due to its left and right side adjustment

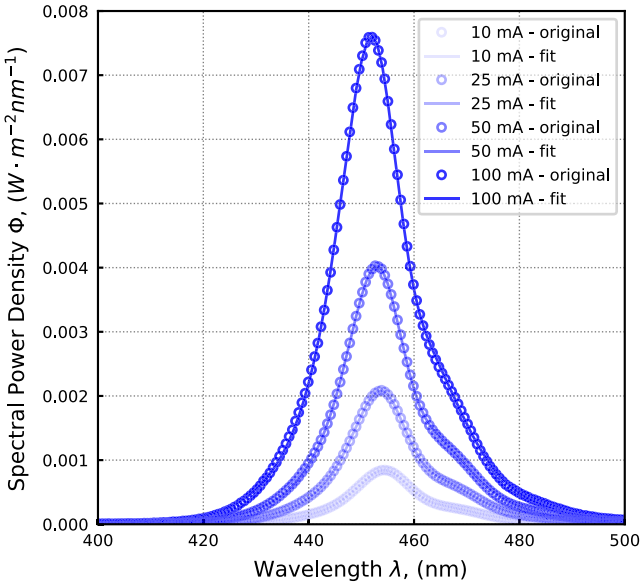

FIGURE 3. Spectral power distribution of a blue monochromatic LED sample for different forward currents I_F: (round markers) Measured SPD and (solid line) fitted SPD with $n = 2$ superimposed *Split Pearson VII* model functions.

parameters $\sigma_1, \sigma_2, S_1, S_2$ adding more fit flexibility compared to a non-split *Pearson VIIb* model.

V. APPLICATION EXAMPLE

This section presents an use case of the above proposed *Pearson VII* model for monochromatic LED spectra. Therefore, a spectral measurement of a blue LED (type: Blue 1) at different forward currents of $I_\mathrm{F} = [10, 25, 50, 100]$mA in an temperature controlled setup was conducted at $T_\mathrm{j} \approx 25\,^\circ$C. This example was specifically chosen due to the unsymmetrical shape of the SPD with a "bump" at around $\lambda \approx 465$ nm to add additional complexity. The measured SPD for each forward current was subsequently fitted with a $n = 2$ function *Split Pearson VII* model. With a $\Delta u'v' \leq 0.001$, $|\Delta\Phi| < 0.2\%$ and $R^2 \geq 0.999$ the applied model yields a very high accuracy for all forward currents. The original SPD and the fitted SPD are shown in figure 3.

Further it should be noted, that the following analysis is intended to show the possibilities and limitations of this approach rather than building a correct physical model. For this model the linear correlation is evaluated. A linear correlation $|r(I_\mathrm{F}, p(I_\mathrm{F}))| \to 1$ indicates a positive or negative linear proportionality between I_F and the functions parameter p. The dependency of each parameter and their linear correlation coefficients are shown in tab. 8 with f_1 and f_2 representing the left and right superimposed functions. The following expectations based on Schubert *et al.* [3] can be evaluated:

1) $I_\mathrm{F} \propto A, \sigma_1, \sigma_2$: As more photons are emitted with increasing forward current and thus increasing the SPDs amplitude as well as its standard deviation σ. σ can be related to the Full Width Half Maximum (FWHM) of the SPD by $FWHM(\sigma) = k\sigma$ where

TABLE 8. Forward current dependency of *Split Pearson VII* model parameters $p(I_F)$ with two superimposed model functions f_1 and f_2 by means of their correlation $r(I_F, p)$.

Parameter p	$r(I_F, p)$ (a.u.)	
	Function f_1	Function f_2
Amplitude (A)	0.999	0.999
Peak wavelength (λ_p)	-0.986	-0.989
Left side standard deviation (σ_1)	0.997	0.630
Right side standard deviation (σ_2)	0.988	0.992
Left side skew factor (S_1)	0.990	0.611
Right side skew factor (S_2)	-0.107	0.984

$k = 2\sqrt{2\ln 2}$ in case of a *Gaussian* distribution function [3]. Both functions yield a high correlations for A, σ_1 and σ_2 except σ_1 of f_2. The reason here can be found in the minimal variation of the left split of f_2 since f_2 mainly contributes to shape of the SPDs right side bump.

2) $I_F \propto \lambda_p^{-1}$: With increasing I_F the SPD shifts to lower peak wavelengths λ_p due to piezoelectric field screening [26], [27]. This effect can also be confirmed by both functions parameters λ_p.
3) $I_F \propto S_1, S_2$: Analyzing the shape of the four example spectra three areas are of interest: The SPDs slope left to $\lambda < \lambda_p$ (a), the right sides slope from the SPDs peak to its bump $\lambda_p \geq \lambda_{bump}$ (b) and lastly the right side bumps prominence (c). Regarding the parameter S_1 table 8 shows a high correlation for f_1 and a mediocre correlation for f_2 since f_1 mainly affects the above described area (a). Similar, f_2 controls the areas (b) and (c) by the parameter S_2. The low correlation of functions f_1 parameter S_2 occurs since the fit algorithm tries to model the right split of f_1 to fit around the bump modeled by f_2. This point clearly shows potential for optimization. One solution can be implementing so called expression models [19] for each parameter to follow a certain physical function.

VI. CONCLUSION AND FUTURE WORK

In this work the least squares fitting performance of different probability density function models on monochromatic and phosphor-converted LED spectra was evaluated. A total of 19 different model functions was examined with $n = 1..3$ and $n = 2..6$ superimposed functions of the same type on seven monochromatic and eight pc-LED spectra respectively. A literature research demonstrated that the coefficient of determination as a goodness of fit metric has a low information value since an $R^2 \geq 0.95$ for the majority of cases was reported. A combination of the change in chromaticity $\Delta u'v'$ and radiant flux $\Delta\Phi$ as well as the Bayesian Information Criterion proved to be more meaningful in mathematical terms and in accordance with the human light perception. As a key result it was concluded that a *(Split) Pearson VII* model function yields highly accurate results on the evaluated SPD sample set contrary to the commonly used *Gaussian* model function. A promising usability of a *(Split) Pearson VII* distribution to model the current dependency of a blue LED was furthermore presented. Thus, this works recommends the *(Split) Pearson VII* model function for the purpose of spectral modeling and decomposition. However, in this work a globally set of fit parameter constraints was applied to all functions. Fitting results may be further improved by determining model specific constraints and starting parameters. In addition, as discussed before the origin of difference of the three Pearson Type VII model functions *VIIa, VIIb, Split VII* has to be examined in depth.

REFERENCES

[1] *CIE 015:2018 Colorimetry*, 4th ed., Int. Commission Illumination, Vienna, Austria, Oct. 2018.
[2] S. Benkner, S. Babilon, A. Herzog, and T. Q. Khanh, "Combined methodology for accurate evaluation of distance and direction of chromaticity shifts in LED reliability tests," *IEEE Trans. Device Mater. Rel.*, vol. 21, no. 4, pp. 500–507, Dec. 2021.
[3] E. F. Schubert, *Light-Emitting Diodes*, 2nd ed. Cambridge, U.K.: Cambridge Univ. Press, 2006.
[4] F. Reifegerste and J. Lienig, "Modelling of the temperature and current dependence of LED spectra," *J. Light Vis. Environ.*, vol. 32, no. 3, pp. 288–294, 2008.
[5] R. Supronowicz and I. Fryc, "The LED spectral power distribution modelled by different functions—How spectral matching quality affected computed LED color parameters," in *Proc. 2nd Balkan Junior Conf. Lighting*, Sep. 2019, pp. 1–4.
[6] A. Keppens, W. R. Ryckaert, G. Deconinck, and P. Hanselaer, "Modeling high power light-emitting diode spectra and their variation with junction temperature," *J. Appl. Phys.*, vol. 108, no. 4, 2010, Art. no. 043104.
[7] M. E. Raypah, M. Devarajan, and F. Sulaiman, "Modeling spectra of low-power SMD LEDs as a function of ambient temperature," *IEEE Trans. Electron Devices*, vol. 64, no. 3, pp. 1180–1186, Mar. 2017.
[8] D. Mozyrska and I. Fryc, "Approximation of spectroradiometric data by fractional model," *Przeglad Elektrotechniczny*, vol. 87, no. 2, pp. 255–257, 2011.
[9] A. Vaskuri, H. Baumgartner, P. Kärhä, G. Andor, and E. Ikonen, "Modeling the spectral shape of InGaAlP-based red light-emitting diodes," *J. Appl. Phys.*, vol. 118, no. 20, Nov. 2015, Art. no. 203103.
[10] A. Vaskuri, P. Kärhä, H. Baumgartner, O. Kantamaa, T. Pulli, T. Poikonen, and E. Ikonen, "Relationships between junction temperature, electroluminescence spectrum and ageing of light-emitting diodes," *Metrologia*, vol. 55, no. 2, pp. 86–95, Mar. 2018.
[11] Z. Guo, T. Shih, Y. Gao, Y. Lu, L. Zhu, G. Chen, Y. Lin, J. Zhang, and Z. Chen, "Optimization studies of two-phosphor-coated white light-emitting diodes," *IEEE Photon. J.*, vol. 5, no. 2, Apr. 2013, Art. no. 8200112.
[12] B.-M. Song and B. Han, "Spectral power distribution deconvolution scheme for phosphor-converted white light-emitting diode using multiple Gaussian functions," *Appl. Opt.*, vol. 52, no. 5, pp. 1016–1024, Feb. 2013.
[13] W. Chen, J. Fan, C. Qian, B. Pu, X. Fan, and G. Zhang, "Reliability assessment of light-emitting diode packages with both luminous flux response surface model and spectral power distribution method," *IEEE Access*, vol. 7, pp. 68495–68502, 2019.
[14] H. Chen and S. Y. Hui, "Dynamic prediction of correlated color temperature and color rendering index of phosphor-coated white light-emitting diodes," *IEEE Trans. Ind. Electron.*, vol. 61, no. 2, pp. 784–797, Feb. 2014.
[15] J. Fan, M. G. Mohamed, C. Qian, X. Fan, G. Zhang, and M. Pecht, "Color shift failure prediction for phosphor-converted white LEDs by modeling features of spectral power distribution with a nonlinear filter approach," *Materials*, vol. 10, no. 7, p. 819, Jul. 2017.
[16] J. Fan, W. Chen, W. Yuan, X. Fan, and G. Zhang, "Dynamic prediction of optical and chromatic performances for a light-emitting diode array based on a thermal-electrical-spectral model," *Opt. Exp.*, vol. 28, no. 9, pp. 13921–13937, Apr. 2020.
[17] J. Fan, Y. Li, I. Fryc, C. Qian, X. Fan, and G. Zhang, "Machine-learning assisted prediction of spectral power distribution for full-spectrum white light-emitting diode," *IEEE Photon. J.*, vol. 12, no. 1, pp. 1–18, Feb. 2020.

[18] C. Qian, J. Fan, X. Fan, and G. Zhang, "Prediction of lumen depreciation and color shift for phosphor-converted white light-emitting diodes based on a spectral power distribution analysis method," *IEEE Access*, vol. 5, pp. 24054–24061, 2017.
[19] M. Newville *et al.*, "lmfit/lmfit-py: 1.0.3," Zenodo, Version 1.0.3, Oct. 2021. [Online]. Available: https://zenodo.org/record/5570790/export/hx, doi: 10.5281/zenodo.5570790.
[20] H.-T. Chen, W. C. H. Choy, and S. Y. Hui, "Characterization, modeling, and analysis of organic light-emitting diodes with different structures," *IEEE Trans. Power Electron.*, vol. 31, no. 1, pp. 581–592, Jan. 2016.
[21] X. Shen, H. Chen, J. Lin, Y. Li, H. Lin, J. Chen, and C. Chen, "Analysis and modeling of optical and thermal properties of phosphor converted white light emitting diode," *IEEE Access*, vol. 7, pp. 118679–118689, 2019.
[22] G. Schwarz, "Estimating the dimension of a model," *Ann. Statist.*, vol. 6, no. 2, pp. 461–464, 1978.
[23] W. Hu and W. Davis, "Dimming curve based on the detectability and acceptability of illuminance differences," *Opt. Exp.*, vol. 24, no. 10, pp. A885–A897, May 2016.
[24] *Chromaticity Difference Specification for Light Sources*, document CIE TN 001:2014, 2014.
[25] *Projecting Long-Term Chromaticity Coordinate Shift of LED Packages, Arrays, and Modules*, document ANSI/IES TM-35-19+E1, 2019.
[26] H. Itoh, S. Watanabe, M. Goto, N. Yamada, M. Misra, A. Y. Kim, and S. A. Stockman, "Current dependence of in-plane electroluminescence distribution of $In_xGa_{1-x}N$/GaN multiple quantum well light emitting diodes," *Jpn. J. Appl. Phys.*, vol. 42, no. 10, pp. L1244–L1247, Oct. 2003.
[27] A. Herzog, M. Wagner, and T. Q. Khanh, "Efficiency droop in green InGaN/GaN light emitting diodes: Degradation mechanisms and initial characteristics," *Microelectron. Rel.*, vol. 112, Sep. 2020, Art. no. 113792.

SIMON BENKNER received the B.Sc. and M.Sc. degrees in electrical engineering from the Technical University of Darmstadt, Germany, in 2015 and 2017, respectively, where he is currently pursuing the Ph.D. degree with the Laboratory of Adaptive Lighting Systems and Visual Processing. He is also working as a Research Assistant at the Laboratory of Adaptive Lighting Systems and Visual Processing, Technical University of Darmstadt. His research interest includes the reliability analysis of light-emitting diodes by applying physical and data driven models to increase lifetime prediction accuracy. In addition, he engages in research on smart lighting systems and digital twins in the context of lighting applications.

ALEXANDER HERZOG was born in Offenbach, Germany, in 1987. He received the B.S., M.S., and Ph.D. degrees in electrical engineering from the Technical University of Darmstadt, in 2012, 2015, and 2020, respectively. He currently works as a Postdoctoral Researcher at the Laboratory of Adaptive Lighting Systems and Visual Processing, Technical University of Darmstadt. His research interests include lifetime prediction, reliability analysis, digital twins of light-emitting diodes, temporal light artefacts, and spectral optimization of metameric spectra.

STEFAN KLIR received the M.Sc. degree in the field of electrical engineering and information technology from the Technical University of Darmstadt, Germany, in 2017, where he is currently pursuing the Ph.D. degree with the Laboratory of Adaptive Lighting Systems and Visual Processing. His research interests include the development of intelligent, and data-driven lighting control systems for integrative lighting applications and to enhance individual user preference.

WILLEM D. VAN DRIEL received the degree in mechanical engineering from the Technical University of Eindhoven and the Ph.D. degree from the Delft University of Technology, The Netherlands. He is currently a Fellow Scientist at Signify (formerly Philips Lighting). Besides that, he is also a Professor at the Delft University of Technology, The Netherlands. He has more than 25 year track record in the reliability domain. Application areas range from healthcare, gas and oil explorations, and semiconductors. He has authored or coauthored more than 350 scientific publications, including journals and conference papers, books or book chapters, and invited keynote lectures. His research interests include solid state lighting, microelectronics and microsystems technologies, virtual prototyping, virtual reliability qualification, and designing for reliability of microelectronics and microsystems. He is the Chair of the Organizing Committee of the IEEE Conference EuroSimE.

TRAN QUOC KHANH received the Dr.-Ing. degree in physics and technology of electronic components and the Habilitation degree in mechanical engineering and technical optics from the Institute for Lighting Technology, Technical University of Illmenau, Germany, in 1989 and 2005, respectively. Since 2006, he has been a Full Professor and the Head of the Laboratory of Adaptive Lighting Systems and Visual Processing, Technical University of Darmstadt, where he has been working as the Dean for the Department of Electrical Engineering and Information Technology, since 2018. He leads research groups in the field of automotive lighting, human-centric lighting, smart indoor lighting, and LED technology.